HHS Public Access

Author manuscript

ACS Infect Dis. Author manuscript; available in PMC 2022 March 12.

Published in final edited form as:

ACS Infect Dis. 2021 March 12; 7(3): 598–607. doi:10.1021/acsinfecdis.0c00765.

Biopolymer Patterning-Directed Secretion in Mucoid and Non-Mucoid Strains of *Pseudomonas aeruginosa* Revealed by Multimodal Chemical Imaging

Jin Jia[†,⊥], **Joanna F. Ellis**[‡,⊥], **Tianyuan Cao**[†], **Kaiyu Fu**[†], **Nydia Morales-Soto**[§], **Joshua D. Shrout**[§,&], **Jonathan V. Sweedler**[‡], **Paul W. Bohn**[*,†,£]

[†] Department of Chemistry and Biochemistry, University of Notre Dame, Notre Dame, Indiana 46556, United States

[£] Department of Chemical and Biomolecular Engineering, University of Notre Dame, Notre Dame, Indiana 46556, United States

[‡] Department of Chemistry and Beckman Institute for Advanced Science and Technology, University of Illinois at Urbana−Champaign, Urbana, Illinois 61801, United States

[§] Department of Civil and Environmental Engineering and Earth Sciences, University of Notre Dame, Notre Dame, Indiana 46556, United States

[&] Department of Biological Sciences, University of Notre Dame, Notre Dame, Indiana 46556, United States

Abstract

Quinolone, pyocyanin, and rhamnolipid production are studied in *Pseudomonas aeruginosa* by spatially patterning mucin — a glycoprotein important to infection of lung epithelia. Mass spectrometric imaging and confocal Raman microscopy are combined to probe *P. aeruginosa* biofilms from mucoid and non-mucoid strains, grown on lithographically-defined patterns. Quinolone signatures from biofilms on patterned *vs.* unpatterned and mucin *vs.* mercaptoundecanoic acid, MUA, surfaces are compared. Microbial attachment is accompanied by secretion of 2-alkyl-4-quinolones as well as rhamnolipids from the mucoid and non-mucoid strains. Pyocyanin is also detected both in the biofilm and in the supernatant in the mucoid strain only. Significant differences in the spatiotemporal distributions of secreted factors are observed between strains and among different surface patterning conditions. The mucoid strain is sensitive to composition and patterning while non-mucoid is not, and in promoting community development

[*]**Corresponding Author:** pbohn@nd.edu. Tel.: +1 574 631 1849. Fax: +1 574 631 8366.

[⊥]AUTHOR CONTRIBUTIONS

Jin Jia and Joanna F. Ellis contributed equally to this work.

Notes

The authors declare no competing financial interest.

ASSOCIATED CONTENT

Supporting Information

The Supporting Information is available free of charge. Tables listing characteristic features of biomolecules detected by CRM and MALDI FT-ICR imaging, optical images of biofilm growth, false-color ion images for selected AQs present during *P. aeruginosa* biofilm formation on patterned mucin at 48 hrs, false-color ion images for selected rhamnolipids present during *P. aeruginosa* biofilm formation on patterned mucin at 48 hrs.

in the mucoid strain, non-patterned surfaces are better than patterned, and mucin is better than MUA. Also, the mucoid strain secretes the virulence factor pyocyanin in a way that correlates with distress. A change in the relative abundance for two rhamnolipids is observed in the mucoid strain during exposure to mucin, whereas minimal variation is observed in the non-mucoid strain. Differences between mucoid and non-mucoid strains are consistent with their strain-specific phenology, in which the mucoid strain develops highly protected and withdrawn biofilms that achieve PQS production under limited conditions.

Graphical Abstract

Raman- and mass spectrometry-based chemical imaging are used to elucidate the spatial and temporal distributions of signaling molecules elicited by substrate patterning. Mucoid and non-mucoid strains of *Pseudomonas aeruginosa* respond differently to surface patterning and the presence of the glycoprotein, mucin.

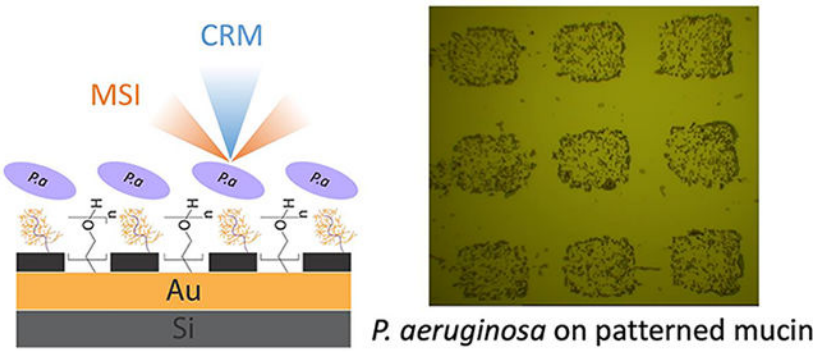

Keywords

biofilm; mass spectrometry; *Pseudomonas aeruginosa*; quorum sensing; Raman spectroscopy

Pseudomonas aeruginosa is a Gram-negative bacterium and opportunistic pathogen responsible for over 50-thousand nosocomial infections in the United States every year, with 13% of the infections exhibiting multidrug resistance.[1] This bacterium is able to regulate a subset of its genes using a density-based, community-wide communication process, termed quorum sensing (QS), which improves resistance to adverse stressors, in part, by signaling bacteria to generate molecules utilized for biofilm development.[2–3] The ability of *P. aeruginosa* to regulate over 10% of its genomic expression in a manner that depends on its neighbors facilitates the adaptation of this pathogen to its surrounding environment, thereby increasing the threat to human health.[4] *P. aeruginosa* QS-based gene regulation utilizes production and sensing of small molecule autoinducers, such as acyl-homoserine lactones and Pseudomonas quinolone signal (PQS).[5–6] As the cellular density of *P. aeruginosa* increases, QS molecules reach a threshold concentration, after which QS regulators are induced that affect biofilm formation, virulence, and other vital survival functions.[7] During biofilm formation, bacterial cells attach to a surface and begin secretion of extracellular polymeric substances (EPS) — a complex mixture of exopolysaccharides, extracellular DNA, and proteins that envelop the attached bacteria.[8–9] EPS displays many impermeable

traits, thereby creating both a physical and chemical barrier and reducing the efficacy of antimicrobial agents and biocides up to 10-fold when compared to planktonic cultures.[10] Complicating this picture is the observation that *P. aeruginosa* strains isolated from cystic fibrosis (CF) patients commonly exhibit a mucoid phenotype caused by overproduction of one particular extracellular polysaccharide, alginate.[11–14]

Mucins are large, extracellular glycoproteins ranging in size from 10 to 300 nm which are found ubiquitously in mammals notably including in CF airways and damaged airway epithelia.[6, 15–18] It is known that *P. aeruginosa* interaction with mucins leads to faster irreversible attachment to surfaces and increased antibiotic tolerance.[7] However, the onset and influence of QS upon the aggregate biofilm phenotype that results from interaction with mucin-containing surfaces of CF airways, is largely uncharacterized. While there are several documented QS pathways in bacteria and the Pseudomonads, the PQS QS pathway is unique to *P. aeruginosa*, and it has been shown to influence virulence and biofilm development in addition to other traits.[19–21] However, the C_7 (2-alkyl-3-hydroxy-4(1*H*)-quinolone) and C_9 (2-heptyl-3-nonyl-4(1*H*)-quinolone) forms of PQS are just two of over 50 alkyl quinolones (AQs) such as 2-heptyl-4(1H)-quinolone (HHQ) and 2-heptyl-4-hydroxyquinoline N-oxide (HQNO)—along with their C_9 side chain variants, NHQ, NQNO,—known to be produced by *P. aeruginosa*.[22] While it is known that HHQ and PQS influence the production of pyocyanin in *P. aeruginosa* via the PqsR and PqsE pathways, and rhamnolipids are controlled by acylhomoserine lactone-based QS, it is not well understood how production of such virulence factors is controlled by mucoid and non-mucoid strains, particularly in three-dimensional environments.[23] Furthermore, pyocyanin is a redox-active species—it is secreted under select conditions and is vital for establishing long-term lung infections and survival in oxygen-poor environments.[24]

Biofilms often manifest as small closely-associated aggregates that display nonrandom spatial organization,[25] and during the last two decades, the spatial coordination of various relevant biological molecules has begun to be specifically investigated.[26] Printing adhesive patterns, fabricating reaction chambers, and developing other microscale tools commensurate in size with individual bacterial cells and bacterial aggregates have helped reveal important relationships between these systems and the spatial structure of their environments.[26–27] For example, researchers have used micro-structuring techniques to pattern bacteria and study how they adapt to different regions of the landscape.[28–30] Studies of synthetically patterned biofilms have demonstrated the importance of interactions among bacterial cell clusters, specifically their structural organization and the size and distance between them.[19–21, 26] However, prior studies have primarily used morphological tools, like AFM, fluorescence microscopy, and SEM,[19, 31–33] to study the response of microbes to the patterns, and these approaches do not yield the molecular information needed to connect spatial organization of cell clusters and QS.

In order to address questions of spatial organization and chemical environment, in the present work we utilize a patterned biopolymer model and apply two complementary chemical imaging approaches – mass spectrometry imaging (MSI)[34] and confocal Raman microscopy (CRM)[35–36] – to probe biofilm signatures for *P. aeruginosa*. MSI enables 2- and 3-D microscale untargeted surface chemical imaging for a wide range of specific molecular

species, complementing CRM which provides information about molecular vibrations. CRM is label-free and non-disruptive for sample analysis, while MSI needs further sample preparation (*e.g.* dehydration, matrix application) and vacuum compatibility. Additionally, imaging by tandem MS was used to further distinguish isomers of AQs present at *m/z* 260.1696 and *m/z* 288.1958 by fragmentation patterns respective to each parent ion, as has been demonstrated in previous work.[37–39] Both MSI and CRM have been applied to studies exploring infectious disease.[40–41] Furthermore, the use of lithographically-defined surface composition patterns makes it possible to compare microbial behavior as a function of patterning (patterned or unpatterned) and composition (mercaptoundecanoic acid, MUA, or mucin), as we have done for one EPS-overproducing mucoid strain, *P. aeruginosa* FRD1, and a non-mucoid strain, *P. aeruginosa* PAO1C. Multimodal imaging by CRM and MSI enable observation of secreted 2-alkyl-4-quinolones, as well as rhamnolipids and pyocyanin (in FRD1 only), in later biofilms. The information-rich chemical imaging approaches used here allow us to study the importance of molecular spatial organization in initial seeding and development of bacteria biofilms, especially the chemical signals that are used by *P. aeruginosa* to coordinate these community-level behaviors. For example, we find that mucoid biofilm formation is accelerated on mucin relative to MUA or bare gold and impeded by patterning on either mucin or MUA. In contrast, non-mucoid AQ profiles are relatively insensitive to substrate composition. The overall AQ and specific PQS responses of these two *P. aeruginosa* strains to constrained surface patterns also demonstrates the rich information that can be gained from multimodal chemical imaging.

RESULTS AND DISCUSSION

Development and Characterization of Mucin-modified Si Substrates.

To isolate specific attributes of bacteria-surface interaction, we studied five surface derivatization conditions: (1) uniform (*i.e.* non-patterned) MUA, (2) uniform (*i.e.* non-patterned) mucin, (3) patterned MUA (P-MUA), (4) patterned mucin (P-Mucin), and (5) underivatized Au. These surfaces allow us to compare patterned *vs.* unpatterned (MUA or mucin) and MUA *vs.* mucin (patterned or unpatterned), and underivatized Au was used as a universal control. The preparation methods for P-MUA and P-Mucin surfaces are shown schematically in Figure 1 and described in the Experimental Section (Supporting Information, SI). Representative optical images of non-mucoid *P. aeruginosa* cells (PAO1C) grown on 100 μm × 100 μm P-mucin pads separated by 100 μm in minimal-glucose versus lysogeny broth (LB) media are shown in Figures S1a and S1b, respectively, confirming the success of the surface modification strategy. After 1 h growth, most samples had developed significantly into the biofilm state. This was confirmed by: (*a*) the morphological appearance of the bacterial structures in normal light microscopy, as shown in Figures S2 and S3, (*b*) the absence of spectral features characteristic of planktonic *P. aeruginosa* cells in CRM, and (*c*) the dominance of spectral features associated with secreted factors during quorum sensing, such as AQs.[42–43]

Mucins constitute a large heterogeneous family of high molecular mass glycoproteins, which can span tens to hundreds of nanometers in length.[44] Given their structural and organizational diversity, mucins cannot easily be oriented in surface layers by site-specific

covalent immobilization, in contrast with smaller proteins.[45–46] However, mucins can be directed to display anisotropic structures at surfaces by manipulating the hydrophobicity/hydrophilicity of the substrate. Hydrophobic surfaces promote the adsorption of glycan-free portions of the mucin protein backbone, so modifying the surface to render it hydrophobic can direct the glycan-containing segments to orient primarily away from the surface, thereby achieving a degree of polar order. Characterizing mucin-derivatized surfaces via CRM is challenging, because they are only weakly scattering, and no detectable mucin peaks were observed in the Raman fingerprint region. Consistent with this, we did not observe ions that localized to the mucin patches by MALDI MSI.[47] However, buckminsterfullerene (C_{60}) SIMS – a harder ionization source – produced fragments at *m/z* 554.8 and *m/z* 608.9, as shown in Figure S1c, that can be attributed to mucin patches and PEG, respectively. We subsequently characterized a non-patterned, mucin-modified surface by SEM and observed particles smaller than 120 nm, Figure S1d, whereas larger mucin particle aggregates were observed at longer incubation times. In comparison, the MUA-functionalized and bare Au surfaces were indistinguishable under SEM.

Detection and Characterization of AQs by CRM, C_{60}-SIMS and MALDI FT-ICR.

In order to assess the role of spatial organization in QS, we surface patterned mucin-defined corrals as shown in Figures 1 and S1 and profiled these, along with bacterial and commercial standards, by CRM, C_{60}-SIMS, and MALDI FT-ICR to determine the signal molecules produced by two distinct strains, PAO1C and FRD1, of surface-confined *P. aeruginosa* cells: *P. aeruginosa* PAO1C, originally a wound isolate,[48] and *P. aeruginosa* FRD1, originally a sputum isolate from a cystic fibrosis patient, which is a mucoid strain that overproduces the exopolysaccharide alginate.[12]

A representative set of CRM data acquired from various *P. aeruginosa* samples is shown in Figure 2. By comparing features in the Z score loadings (*top row*) from biofilms with vibrational spectra acquired from standards, three molecular classes were identified in bacterial samples by CRM: 2-nonyl/heptyl-4-hydroxyquinoline N-oxide (N/HQNO), 2-nonyl/heptyl-3-hydroxy-4-quinolone (PQS), and pyocyanin (PYO). Z-score plots corresponding to principal components dominated by these three molecular species are shown across the top row of Figure 2, and characteristic features for these species are given in Table S1 and compared to the positions of Raman bands in standards. Two important points amplify the independent origins of these spectral signatures. First, the z-score plots—which resemble Raman spectra—are distinct for all three specified components. All exhibit a strong feature in the 1330–1380 cm^{-1} region occupied by bands assigned to the quinolone ring stretch and pyocyanin marker band. Even though the center positions for this characteristic feature vary by only a few cm^{-1} among the three components (1360 cm^{-1}, 1376 cm^{-1}, 1357 cm^{-1}), respectively, they are easily resolved spectrally at high precision. In addition, visual inspection of the Z-score plots in the top row of Figure 2 and the feature positions in Table S1, clearly reveal that the pattern of features for each of the putative secreted molecules is distinct, making it possible to associate a particular group of features with the specific conditions used to obtain it. For example, features which map onto the Raman spectrum of HQNO are prevalent in the 24h PAO1C biofilm on Au, while PQS-like features dominate the 48 h PAO1C biofilm on mucin. Finally, comparison of the relative

intensities of spectral and Z score features, such as the distinctive closely-spaced pair of bands at 681/715 cm^{-1} in Figure 2(A) and in the H/NQNO standard add confidence to the assignments.

Further characterization of the components observed under these sets of conditions used MALDI FT-ICR-MS, in which we detected and separated each AQ with a combination of high-resolution spectral acquisition and imaging with resolving powers 530,000 and 125,000 at *m/z* 123 and *m/z* 137, respectively, and tandem mass spectrometry. Using fragments at *m/z* 159.0679 and *m/z* 175.0628 for N-Oxide- and PQS-type AQs, respectively, we were able to separate the isomeric species as shown by the full list of compounds targeted in the static biofilms in Table S2 and the single component spectra shown in Figure S4.

Initial characterization used four time-points starting at 1 h. HHQ, the immediate PQS precursor,[49–50] was detected in 1h samples of both FRD1 and PAO1C strains by SIMS imaging, as HHQ is easily ionized by SIMS even at very low concentrations,[39] but not by CRM or MALDI MSI. Only the 24 h and the 48 h FRD1 and PAO1C samples exhibited signals characteristic of all AQs of interest above the limit of detection (LOD) in all three imaging modalities – CRM, SIMS and MALDI MSI, *viz.* Figure S5 – so the subsequent analysis focused on these two time-points. In addition to AQs, Figure S6 shows that rhamnolipids were observed in the 24 and 48 h samples for both *P. aeruginosa* strains, with PAO1C biofilms exhibiting both more rhamnolipid content and more diverse chain length and saturation than those resulting from FRD1.

Mucin Interaction and Patterning Affect Onset of Late Biofilm Signatures in the Mucoid Strain.

Multimodal imaging experiments revealed that mucoid and non-mucoid strains display markedly different behavior on the five surfaces. CRM spectral signatures obtained from imaging data, such as that shown in Figure 2, are summarized for all five surfaces at ≤ 7 h, 24 h, and 48 h in Table 1. At early times, none of the *P. aeruginosa* samples secreted sufficient AQs to be observable. However, starting at 24 h, interesting, surface-dependent effects were observed, involving the mucoid strain FRD1. Specifically, distinct Raman scattering signatures were observed between the patterned (no AQs, only salt) and unpatterned (HQNO) MUA and between P-Mucin (HQNO) and P-MUA (only salt). Furthermore, the virulence factor pyocyanin was observed on the Au control surface. Given that HQNO is a precursor to the chemical signal PQS, these results suggest that activity of the mucoid strain is hindered by P-MUA, but not by P-Mucin. In addition, the secretion of pyocyanin by the mucoid strain on bare Au suggests that it is perceived as a hostile environment. In contrast, the non-mucoid strain, PAO1C, is agnostic to surface composition and pattering at 24 h. At 48 h, while the non-mucoid strain was similarly agnostic, secreting both HQNO and PQS independent of surface composition and patterning, FRD1 samples evolved further to exhibit a variety of surface-dependent secretion patterns. The late biofilm signature PQS is observed on Mucin, P-Mucin, and MUA, but not on P-MUA or bare Au. The virulence factor PYO is observed on both patterned and unpatterned MUA and bare Au, but not on either mucin surface. A typical progression during *P. aeruginosa* community development proceeds by initial appearance of N/HQNO and then PQS. MALDI FT-ICR

MSI confirmed the tentative conclusions from CRM by showing an overall increase in PQS-type AQs in the 24 h and 48 h mucoid strain samples grown on patterned or unpatterned mucin compared to MUA or the Au-control. These results indicate that FRD1 mucoid strain biofilm development is accelerated on mucin relative to MUA or bare gold surfaces. Clearly, both MSI and CRM data indicate that mucin promotes the formation and development of mature mucoid biofilms on mucin-containing surfaces and the early onset of the N/HQNO→PQS progression.[51–52]

In addition, PYO, which was observed in mucoid FRD1 samples under various conditions, is never detected from PAO1C samples, which is consistent with previous observations.[53] In addition to the patterned and unpatterned substrates, Raman microspectroscopy was also applied to pellicle biofilms formed at the air-water interface and to the supernatant solution above the solid surface. PYO was detected in both the pellicle biofilm and the supernatant above the mucoid strain grown on MUA at both 24 h and 48 h. Interestingly, static biofilms of mucoid FRD1 on MUA exhibit only N/HQNO at 24 h, suggesting that PYO is associated with the presence of the pellicle biofilm in these samples.

As noted above, non-mucoid PAO1C samples uniformly exhibit N/HQNO at 24 h, and both N/HQNO and PQS at 48 h on all patterned and non-patterned surfaces by CRM, Table 1. The relative insensitivity of non-mucoid strain profiles to substrate composition indicates that biofilm formation in the non-mucoid strain is more robust than that of the mucoid strain. To further elucidate the relative signal levels of different AQs produced by both types of biofilms on MUA and mucin surfaces, MSI data displayed in Figure 3 indicate lower amounts of C_7-congeners, HHQ and HQNO, and higher amounts of the C_9-species, C_9-PQS and NQNO on mucin surfaces compared to MUA surfaces. This is observed for both mucoid and non-mucoid strains at both 24 h and 48 h (see, for example, inversion of relative signals on Mucin/MUA in 1st and 3rd rows). Certainly these data demonstrate that the relative signal levels of AQs are a useful tool in evaluating *P. aeruginosa* development.

Compositional Patterning Affects Quorum Sensing in *Pseudomonas aeruginosa* Biofilms.

We analyzed the evolution of mucoid and non-mucoid *P. aeruginosa* biofilms on patterned surfaces compared with that on non-patterned surfaces. Morphologically, biofilm formation on patterned surfaces begins with a clear patterned distribution of cells on the surface, as shown in Figure S1. Over time, starting from the initial pattern, cells began to invade the surrounding non-seeded areas, until at 24 h a layer of cells completely covers the substrates, as shown in Figures S2 and S3. These morphological observations frame the chemical imaging experiments, which are intended to elucidate the effects of specific surface compositions and patterns on bacterial signaling and biofilm development.

Mucoid strain samples exhibit N/HQNO on unpatterned MUA at 24 h, but no AQ metabolites at all were detected on P-MUA (Table 1). At 48 h, the mucoid samples show N/HQNO, PQS and PYO on MUA surfaces, while only N/HQNO and PYO were detected on P-MUA. These results indicate that the discrete patterning on P-MUA limits development of mucoid FRD1 biofilms to a mature PQS-inactive state relative to those biofilms that form on unpatterened MUA. In contrast, AQ profiles of non-mucoid PAO1C were largely unaffected by any compositional patterning with or without mucin.

The proportions of C_7/C_9 AQ congeners also varies between the mucoid and non-mucoid strains. MSI results shown in Figure 3 indicate that 24 h and 48 h mucoid samples secrete lower levels of C_9-PQS and NQNO and higher amounts of HHQ and PQS on P-Mucin relative to unpatterned mucin surfaces, which is opposite to the trend observed going from unpatterned mucin to unpatterned MUA. In contrast, the MSI results in Figure 3 for non-mucoid PAO1C show lower amounts of C_7 HHQ and HQNO and higher amounts of C_9-PQS and PQS on P-MUA surfaces compared to unpatterned MUA at both 24 h and 48 h, suggesting that MUA patterning promotes the secretion of these AQs in this non-mucoid strain.

We attribute the differences in response to compositional patterning exhibited by these strains to the dominance of mucoid biofilm influence, when present. FRD1 is a cystic fibrosis lung isolate that hyper-produces alginate, which has long been associated with a highly impervious and recalcitrant chronic disease *P. aeruginosa* biofilm state.[13, 54] The resilience exhibited by these mucoid biofilms necessitates prompt and dedicated isolation from outside influences (both friendly and unfriendly). In contrast, non-mucoid PAO1C appears capable of continued environmental sensing and bridging of gaps, unlike FRD1. This is consistent with our observation that the 100 μm × 100 μm pattern does not impede biofilm development in the non-mucoid strain, instead giving rise to temporal changes in bacterial density in the between-pattern spaces. Moreover, mucoid biofilms form in the respiratory tract, where interaction with host mucins are abundant. To this end, we have also examined differences in chemical signaling (AQs) and remodeling the mechanical properties of the EPS (Rha), in response to composition and patterning.

Mucin Alters Rhamnolipid Composition Differently in Mucoid and Non-mucoid *P. aeruginosa*.

MSI was also applied to selected rhamnolipids known to be present in *P. aeruginosa* biofilms (Figure S7). Similar to the AQ profiles, minimal changes in the overall composition of rhamnolipids were observed for compositional patterning of the non-mucoid strain in the presence of mucin (patterned or unpatterned). In contrast, we observed a general increase in the relative abundance of Rha-C10-C10 and a decrease in Rha-Rha-C10 for the mucoid strain FRD1 at 24 h. Rha-C10-C10 and Rha-Rha-C10 were the most highly produced rhamnolipids observed for the mucoid strain, and while there were fewer variations in composition between conditions in the PAO1C strain, PAO1C exhibited higher abundances of a variety of other rhamnolipids, as can be observed in Figure S6. In this regard, the difference in behavior between mucoid and non-mucoid strains mirrors the general compositional and patterning differences observed by CRM between the strains.

CONCLUSIONS

Well-defined spatial patterns of mucin and MUA have been used to elucidate the combined effect of spatial confinement and surface composition on PQS signal production by *P. aeruginosa* mucoid and non-mucoid strains. Multimodal chemical imaging using CRM, SIMS, and MALDI FT-ICR reveals that production of PQS and other AQs by *P. aeruginosa* bacterial biofilms is strongly affected by composition and spatial patterning of surfaces for

the mucoid, but not for the non-mucoid, strain. In particular, the temporal evolution of chemical signals that are known correlates of biofilm formation and development and which ultimately reflect interactions among bacterial cell clusters that exhibit PQS signaling is strongly affected for the mucoid strain FRD1. Furthermore, a general ordering of conditions promoting development of communities of the mucoid strain was observed, in which: unpatterned > patterned and mucin > MUA, so all other factors being equal the most favorable conditions involve unpatterned mucin, and the least favorable are found with patterned MUA. Finally, the virulence factor PYO is observed in the most hostile environments for the mucoid strain – bare Au at both 24 h and 48 h and patterned and unpatterned MUA at 48 h.

Data from this study highlights how cell-to-cell signaling has the potential to be influenced by spatial distribution, which is important to understand how structural heterogeneity develops in bacterial biofilms. The potential for cluster-cluster interactions in determining the physicochemical properties of biofilms deserves further study. It will be useful to determine the impact of relative distance between bacterial clusters that initiate and develop biofilms to better understand QS signaling within biofilms and how this affects subsequent behavior important to infection. We plan to expand this investigation by researching *P. aeruginosa* response to alternative polymers, functionally-modified mucin patterning, and modified pattern spacing.

METHODS

Materials and Reagents.

Poly(ethylene glycol) (PEG) thiol (MW 550 Da) was purchased from Creative PEGWorks. Tris (2-carboxyethyl) phosphine hydrochloride (TCEP), 2-(N-morpholino)ethanesulfonic acid (MES) hydrate, hydrogen peroxide solution, ethyl alcohol (200 proof), mucin from porcine stomach and 11-mercaptoundecanoic acid (MUA) were purchased from Sigma-Aldrich. EDC (1-ethyl-3-[3-dimethylaminopropyl] carbodiimide hydrochloride) and NHS (N-hydroxysuccinimide) were purchased from Thermo Fisher Scientific. Silicon wafers, 76.2 mm diam., were purchased from University Wafer. Deionized (DI) water was prepared using a Milli-Q Gradient water purification system (Millipore) with a resistivity $\rho \sim 18.2$ MΩ cm at 25°C. Gold, Au, was purchased as 99.999% purity pellets from Kurt J. Lesker. Dulbecco's Phosphate Buffered Saline (PBS, 1x, without calcium and magnesium) was purchased from Lonza. Sylgard 184 Silicone Elastomer Kit was purchased from Dow Corning Corporation. SU-8 2050 and SU-8 Developer were purchased from MicroChem. Photomasks were purchased from Front Range Photomask. All reagents were used as received.

Stamp Fabrication.

Photomasks were designed using the layout editor software L-Edit (Tanner Research). The side width (W) of the square pad pattern was set to 100 μm, and the distance (D) between adjacent patterned pads was set to a constant value of 100 μm. The silicon (Si) wafers were then spin coated with negative SU-8 2050 photoresist to 50 μm thickness (4000 rpm, 60 s) and subsequently soft baked (95°C, 6 min). A patterned shadow photomask was used to

control exposure of the photoresist-coated Si wafer to UV radiation, with cross-linking achieved in unmasked areas by 11s exposure on the Karl SUSS MJB3 contact mask aligner (SUSS Microtec). After exposure, wafers were soft-baked (95°C, 6 min), and the patterned photoresist was developed using SU-8 developer, then rinsed with isopropyl alcohol for 10 s, and dried with N_2. A 10:1 mixture of poly(dimethylsiloxane) (PDMS) prepolymer and curing agent was combined and stirred until thoroughly mixed. PDMS polymer was then poured on the SU-8 photoresist patterned silicon master, degassed in a vacuum desiccator for 1 h, and cured at 65°C for 10 h. After the stamps were peeled from the silicon masters, they were sonicated in ethanol for 1 h and dried with N_2.

Bacterial Substrate Fabrication and Surface Modification.

The general substrate preparation strategy is outlined in Figure 1 of the main text. A (100) silicon (Si) wafer was pretreated in piranha solution (1:3 v:v H_2O_2:H_2SO_4) for 1 h (*Caution - strong oxidizer - use appropriate personal protective gear and work in a properly vented fume hood*). Then, the Si wafer was rinsed with DI water and dried with N_2. Gold (Au) films (50 nm thickness) were coated in a Cressington thermal evaporator (308R, Ted Pella, Inc) using 5 nm chromium (Cr) as an adhesion layer. The Au-coated Si wafer was cleaved into 2 cm × 2 cm tiles and subjected to piranha pretreatment for 1 h and then rinsed with successive aliquots of PBS buffer, ethanol, and DI water, followed by drying with N_2. The patterned PDMS stamp was first inked with MUA (1 mM) then brought into contact with the Au-coated Si substrate for 10 min. The tiles were then incubated in PEG solutions for 16 h. A 5 mM 1:1 mole ratio solution of EDC and NHS was prepared and added to the substrates. After rinsing, mucin solution (1 mg/mL) was drop cast onto the same zones on the substrates and allowed to stand for 4 h. The tiles were cleaned by rinsing with DI water, dried with N_2, and stored in a sterile Petri dish at room temperature until use.

Biofilm Preparation.

P. aeruginosa strains PAO1C (ATCC15692) and FRD1 were used in all experiments. Cultures were grown in minimal medium containing 30 mM filter-sterile glucose as the sole carbon source[43, 51] with shaking at 240 rpm at 37 °C for 18 h. Cultures were then diluted to an OD_{600} = 0.3 in fresh minimal medium. Then, 200 μL of diluted culture was pipetted onto prepared tiles in a Petri dish (each Petri dish holding four tiles). After 10 min for bacterial attachment, the tiles were gently rinsed with Dulbecco Phosphate Buffered Saline twice to remove loosely attached and unattached cells. These inoculated tiles were then fully immersed in 18 mL of fresh minimal-glucose medium and incubated at 37°C for the desired growth time. The tiles were carefully removed from the Petri dish with sterile tweezers, covered, and allowed to air-dry overnight in a fume hood.

Confocal Raman Microscopy (CRM).

An Alpha 300R confocal Raman microscope (WITec Instruments Corp) equipped with a solid-state diode pumped laser (λ = 785 nm) excitation source and 40× (NA = 0.6) objective was used to collect Raman microspectra as a function of *x-y* position from all samples. Six to ten Raman images from biofilms were obtained by collecting a full Raman spectrum at each image pixel (60 × 60 pixels) over a 25 μm × 25 μm region on each sample with an integration time of 100 ms per pixel. CRM imaging was directed by white-light

morphological images to acquire data on the mucin-patterned areas, off the mucin-patterned areas, and at the interfaces between the two. A sum filter (spectral range 1330 $cm^{-1} \leq \Delta\tilde{v} \leq$ 1380 cm^{-1}) was used to obtain Raman chemical images. Software WITec project 2.1 was used to perform data analysis on Raman images. Principal component analysis (PCA) was processed on Raman images in MATLAB (Mathworks Inc.).

Matrix Preparation and MALDI FT-ICR Imaging.

MALDI slides were coated via automatic sprayer with 2,5-dihydoxybenzoic acid (DHB) for a deposition density of approximately 0.30 mg/cm^2. The automatic sprayer is described elsewhere.[55] Post-deposition, sample and substrates were desiccated in a N_2 dry box prior to imaging MALDI MS. Imaging was performed using a MALDI solariX XR 7T FT-ICR mass spectrometer (Bruker Corp, Billerica, MA) in positive ionization mode with a mass window of 50–1000. The minimum laser setting was selected with a laser footprint of approximately 10 μm with 100 μm and 200 μm between stage steps for MS and tandem MS imaging. 250 laser shots were accumulated with a frequency of 1000 Hz at 50% of the maximum laser power. For tandem-MS imaging, parent ions of *m/z* 261.2 and *m/z* 289.2 were isolated with an isolation window of ±2.5 Da and collision energies of 20 eV and 25 eV, respectively. The laser was stepped down 33 μm for subsequent acquisitions to prevent oversampling. Regions of approximately 25 mm × 25 mm were selected in FlexImaging (Bruker Corp.) and acquired with ftmsControl (Bruker Corp.). Data was then processed further in SCiLS Lab (Bruker Corp.), exported as a root-mean-square (RMS) normalized imzML, and remaining analysis performed in MATLAB.

SIMS Imaging.

Biofilms were dehydrated[37] and then imaged with a 20 keV Buckminsterfullerene (C_{60}^+) primary ion beam (Ionoptika Ltd, Chandler's Ford, UK) outfitted on a modified QSTAR XL quadrupole time-of-flight (qTOF) mass spectrometer (AB SCIEX, Framingham, MA, USA). This custom instrument is described in detail in a previous article.[56] A Pelco® 300 Mesh Au TEM grid (Ted Pella Inc, Redding, CA, USA) was used for ion focusing with an ultimate beam spot-size of approximately 8 μm as observed with a secondary electron detector and ions collected from *m/z* 50–850. All ion acquisitions were performed in positive-ion mode. These dehydrated biofilms were initially imaged with a 100 μm raster spacing with the 8 μm primary ion beam generating 200 pA of current for a total ion dosage of 1×10^{14} $ions/cm^2$. False-color ion maps were generated from relative intensities of a selected ion (±0.05 *m/z*) with total ion count normalization during preprocessing.

Scanning Electron Microscopy (SEM).

Samples were prepared for SEM by sputter-coating using a Denton Vacuum Desk II (Moorestown, NJ) operated with 60 mTorr Ar with 40 mA current for 70 seconds for a thickness of approximately 7 nm of Au/Pd. Samples were analyzed with surface modifications using a Philips XL30 ESEM-FEG (Hillsboro, OR) operated under high-vacuum conditions at 10 kV at a working distance of 10 mm.

Data Analysis.

All Raman experiments were repeated on three biological replicates per sample condition per strain with a minimum of 6–10 technical replicates. MALDI FT-ICR-MS data from the same three biological replicates per condition per strain acquired in MS and MS^2 (total of 120 total images) were imported into MATLAB with imzML reader, and specific *m/z* ions were selected within a mass window of ±3 ppm. Intensities for N-oxide-type or PQS-type AQs were scaled by the relative abundance of their fragments at *m/z* 159.0679 or *m/z* 175.0628 that were obtained during tandem MS of the parent isomeric ion as has been used in a previous studies to distinguish HQNO and PQS, along with their 9-carbon variants.[39] A Wilcoxon rank-sum test was performed between datasets normalized to biofilms on their respective Au-coated substrate control to determine the presence of significant changes in analyte abundance between sample conditions ($p < 0.05$). Generation of false-color ion maps was performed in MATLAB with MSiReader[57] with a mass range of ±3 ppm of the selected ion of interest on RMS normalized data exported from Scils Lab (SCiLS GmbH) for FT-ICR.

Supplementary Material

Refer to Web version on PubMed Central for supplementary material.

ACKNOWLEDGMENTS

This work was funded by NIH grant R01 AI113219. J.F.E. acknowledges support from the Springborn Endowment and an ACS Analytical Chemistry Division Graduate Fellowship. Fabrication and characterization of Si masters were accomplished at the Notre Dame Nanofabrication Facility.

REFERENCES

1. Bassetti M; Vena A; Russo A; Croxatto A; Calandra T; Guery B, Rational approach in the management of Pseudomonas aeruginosa infections. Curr. Opin. Infect. Dis. 2018, 31 (6), 578–586. DOI: 10.1097/qco.0000000000000505. [PubMed: 30299364]
2. Davies DG; Parsek MR; Pearson JP; Iglewski BH; Costerton JW; Greenberg EP, The Involvement of Cell-to-Cell Signals in the Development of a Bacterial Biofilm. Science 1998, 280 (5361), 295. DOI: 10.1126/science.280.5361.295. [PubMed: 9535661]
3. Shrout JD; Tolker-Nielsen T; Givskov M; Parsek MR, The contribution of cell-cell signaling and motility to bacterial biofilm formation. MRS Bull. 2011, 36 (5), 367–373. DOI: 10.1557/mrs.2011.67. [PubMed: 22053126]
4. Wagner VE; Bushnell D; Passador L; Brooks AI; Iglewski BH, Microarray analysis of Pseudomonas aeruginosa quorum-sensing regulons: effects of growth phase and environment. J. Bacteriol. 2003, 185 (7), 2080–2095. DOI: 10.1128/jb.185.7.2080-2095.2003. [PubMed: 12644477]
5. Miller MB; Bassler BL, Quorum Sensing in Bacteria. Ann. Rev. Microbiol. 2001, 55 (1), 165–199. DOI: 10.1146/annurev.micro.55.1.165. [PubMed: 11544353]
6. Haley CL; Colmer-Hamood JA; Hamood AN, Characterization of biofilm-like structures formed by Pseudomonas aeruginosa in a synthetic mucus medium. BMC Microbiol. 2012, 12 (1), 181. DOI: 10.1186/1471-2180-12-181. [PubMed: 22900764]
7. Landry RM; An D; Hupp JT; Singh PK; Parsek MR, Mucin–Pseudomonas aeruginosa interactions promote biofilm formation and antibiotic resistance. Mol. Microbiol. 2006, 59 (1), 142–151. DOI: 10.1111/j.1365-2958.2005.04941.x. [PubMed: 16359324]
8. Moradali MF; Ghods S; Rehm BHA, Pseudomonas aeruginosa Lifestyle: A Paradigm for Adaptation, Survival, and Persistence. Front. Cell. Infect. Microbiol. 2017, 7, 39–39. DOI: 10.3389/fcimb.2017.00039. [PubMed: 28261568]

9. Costerton JW; Stewart PS; Greenberg EP, Bacterial Biofilms: A Common Cause of Persistent Infections. Science 1999, 284 (5418), 1318. DOI: 10.1126/science.284.5418.1318. [PubMed: 10334980]

10. Mah T-FC; O'Toole GA, Mechanisms of biofilm resistance to antimicrobial agents. Trends Microbiol. 2001, 9 (1), 34–39. DOI: 10.1016/S0966-842X(00)01913-2. [PubMed: 11166241]

11. Doggett RG, Incidence of Mucoid Pseudomonas aeruginosa from Clinical Sources. Appl. Microbiol. 1969, 18 (5), 936. [PubMed: 4984207]

12. Ohman DE; Chakrabarty AM, Genetic mapping of chromosomal determinants for the production of the exopolysaccharide alginate in a Pseudomonas aeruginosa cystic fibrosis isolate. Infect. Immun. 1981, 33 (1), 142. [PubMed: 6790439]

13. Hentzer M; Teitzel GM; Balzer GJ; Heydorn A; Molin S; Givskov M; Parsek MR, Alginate Overproduction Affects Pseudomonas aeruginosa Biofilm Structure and Function. J. Bacteriol. 2001, 183 (18), 5395. DOI: 10.1128/JB.183.18.5395-5401.2001. [PubMed: 11514525]

14. Bjarnsholt T; Jensen PØ; Fiandaca MJ; Pedersen J; Hansen CR; Andersen CB; Pressler T; Givskov M; Høiby N, Pseudomonas aeruginosa biofilms in the respiratory tract of cystic fibrosis patients. Pediatr. Pulmonol 2009, 44 (6), 547–558. DOI: 10.1002/ppul.21011. [PubMed: 19418571]

15. Kesimer M; Sheehan JK, Mass Spectrometric Analysis of Mucin Core Proteins. Methods Molec. Biol. 2012, 842, 67–79. DOI: 10.1007/978-1-61779-513-8_4. [PubMed: 22259130]

16. Bansil R; Turner BS, Mucin structure, aggregation, physiological functions and biomedical applications. Curr. Opin. Colloid Interface Sci. 2006, 11 (2), 164–170. DOI: 10.1016/j.cocis.2005.11.001.

17. Sriramulu DD; Lünsdorf H; Lam JS; Römling U, Microcolony formation: a novel biofilm model of Pseudomonas aeruginosa for the cystic fibrosis lung. J. Med. Microbiol. 2005, 54 (7), 667–676. DOI::10.1099/jmm.0.45969-0. [PubMed: 15947432]

18. Yakubov GE; Papagiannopoulos A; Rat E; Waigh TA, Charge and Interfacial Behavior of Short Side-Chain Heavily Glycosylated Porcine Stomach Mucin. Biomacromolecules 2007, 8 (12), 3791–3799. DOI: 10.1021/bm700721c. [PubMed: 17979238]

19. Gu H; Hou S; Yongyat C; De Tore S; Ren D, Patterned Biofilm Formation Reveals a Mechanism for Structural Heterogeneity in Bacterial Biofilms. Langmuir 2013, 29 (35), 11145–11153. DOI: 10.1021/la402608z. [PubMed: 23919925]

20. Arnfinnsdottir NB; Ottesen V; Lale R; Sletmoen M, The Design of Simple Bacterial Microarrays: Development towards Immobilizing Single Living Bacteria on Predefined Micro-Sized Spots on Patterned Surfaces. PLOS ONE 2015, 10 (6), e0128162. DOI: 10.1371/journal.pone.0128162. [PubMed: 26039378]

21. Vasudevan R; Kennedy AJ; Merritt M; Crocker FH; Baney RH, Microscale patterned surfaces reduce bacterial fouling-microscopic and theoretical analysis. Colloids Surf. B 2014, 117 (Supplement C), 225–232. DOI: 10.1016/j.colsurfb.2014.02.037.

22. Lépine F; Milot S; Déziel E; He J; Rahme LG, Electrospray/mass spectrometric identification and analysis of 4-hydroxy-2-alkylquinolines (HAQs) produced by Pseudomonas aeruginosa. J. Am. Soc. Mass. Spectrom. 2004, 15 (6), 862–869. DOI: 10.1016/j.jasms.2004.02.012. [PubMed: 15144975]

23. Nadal Jimenez P; Koch G; Thompson JA; Xavier KB; Cool RH; Quax WJ, The Multiple Signaling Systems Regulating Virulence in Pseudomonas aeruginosa. Microbiol. Molec. Biol. Rev. 2012, 76 (1), 46. DOI: 10.1128/MMBR.05007-11. [PubMed: 22390972]

24. Rada B; Leto TL, Pyocyanin effects on respiratory epithelium: relevance in Pseudomonas aeruginosa airway infections. Trends Microbiol. 2013, 21 (2), 73–81. DOI: 10.1016/j.tim.2012.10.004. [PubMed: 23140890]

25. Connell JL; Kim J; Shear JB; Bard AJ; Whiteley M, Real-time monitoring of quorum sensing in 3D-printed bacterial aggregates using scanning electrochemical microscopy. Proc. Natl. Acad. Sci. USA 2014, 111 (51), 18255–18260. DOI: 10.1073/pnas.1421211111. [PubMed: 25489085]

26. Schwarz US; Nelson CM; Silberzan P, Proteins, cells, and tissues in patterned environments. Soft Matter 2014, 10 (14), 2337–2340. DOI: 10.1039/C4SM90028F. [PubMed: 24623042]

27. Hentzer M; Wu H; Andersen JB; Riedel K; Rasmussen TB; Bagge N; Kumar N; Schembri MA; Song Z; Kristoffersen P; Manefield M; Costerton JW; Molin S; Eberl L; Steinberg P; Kjelleberg S;

Høiby N; Givskov M, Attenuation of Pseudomonas aeruginosa virulence by quorum sensing inhibitors. EMBO J. 2003, 22 (15), 3803. [PubMed: 12881415]

28. Weibel DB; DiLuzio WR; Whitesides GM, Microfabrication meets microbiology. Nat Rev Micro 2007, 5 (3), 209–218.
29. Jeong HE; Kim I; Karam P; Choi H-J; Yang P, Bacterial Recognition of Silicon Nanowire Arrays. Nano Letters 2013, 13 (6), 2864–2869. DOI: 10.1021/nl401205b. [PubMed: 23682751]
30. Hansen RH; Timm AC; Timm CM; Bible AN; Morrell-Falvey JL; Pelletier DA; Simpson ML; Doktycz MJ; Retterer ST, Stochastic Assembly of Bacteria in Microwell Arrays Reveals the Importance of Confinement in Community Development. PLOS ONE 2016, 11 (5), e0155080. DOI: 10.1371/journal.pone.0155080. [PubMed: 27152511]
31. Jauvert E; Palleau E; Dague E; Ressier L, Directed Assembly of Living Pseudomonas aeruginosa Bacteria on PEI Patterns Generated by Nanoxerography for Statistical AFM Bioexperiments. ACS Appl. Mater. Interf. 2014, 6 (23), 21230–21236. DOI: 10.1021/am506241n.
32. Yu Q; Cho J; Shivapooja P; Ista LK; Lopez GP, Nanopatterned smart polymer surfaces for controlled attachment, killing, and release of bacteria. ACS Appl. Mater. Interf. 2013, 5 (19), 9295–304. DOI: 10.1021/am4022279.
33. Ma C; Trujillo MJ; Camden JP, Nanoporous Silver Film Fabricated by Oxygen Plasma: A Facile Approach for SERS Substrates. ACS Appl. Mater. Interf. 2016, 8 (36), 23978–84. DOI: 10.1021/acsami.6b08191.
34. Traxler MF; Watrous JD; Alexandrov T; Dorrestein PC; Kolter R, Interspecies Interactions Stimulate Diversification of the Streptomyces coelicolor Secreted Metabolome. Mbio 2013, 4 (4). DOI: 10.1128/mBio.00459-13.
35. Ellis DI; Cowcher DP; Ashton L; O'Hagan S; Goodacre R, Illuminating disease and enlightening biomedicine: Raman spectroscopy as a diagnostic tool. Analyst 2013, 138 (14), 3871–3884. DOI: 10.1039/c3an00698k. [PubMed: 23722248]
36. Ivleva NP; Wagner M; Szkola A; Horn H; Niessner R; Haisch C, Label-Free in Situ SERS Imaging of Biofilms. J. Phys. Chem. B 2010, 114 (31), 10184–10194. DOI: 10.1021/jp102466c. [PubMed: 20684642]
37. Lanni EJ; Masyuko RN; Driscoll CM; Dunham SJB; Shrout JD; Bohn PW; Sweedler JV, Correlated Imaging with C60-SIMS and Confocal Raman Microscopy: Visualization of Cell-Scale Molecular Distributions in Bacterial Biofilms. Anal. Chem. 2014, 86 (21), 10885–10891. DOI: 10.1021/ac5030914. [PubMed: 25268906]
38. Schie IW; Rüger J; Mondol AS; Ramoji A; Neugebauer U; Krafft C; Popp J, High-Throughput Screening Raman Spectroscopy Platform for Label-Free Cellomics. Anal. Chem. 2018, 90 (3), 2023–2030. DOI: 10.1021/acs.analchem.7b04127. [PubMed: 29286634]
39. Dunham SJB; Ellis JF; Baig NF; Morales-Soto N; Cao T; Shrout JD; Bohn PW; Sweedler JV, Quantitative SIMS Imaging of Agar-Based Microbial Communities. Anal. Chem. 2018, 90 (9), 5654–5663. DOI: 10.1021/acs.analchem.7b05180. [PubMed: 29623707]
40. Davies SK; Fearn S; Allsopp LP; Harrison F; Ware E; Diggle SP; Filloux A; McPhail DS; Bundy JG, Visualizing Antimicrobials in Bacterial Biofilms: Three-Dimensional Biochemical Imaging Using TOF-SIMS. mSphere 2017, 2 (4), e00211–17. DOI: 10.1128/mSphere.00211-17. [PubMed: 28744481]
41. Ayala OD; Wakeman CA; Pence IJ; Gaddy JA; Slaughter JC; Skaar EP; Mahadevan-Jansen A, Drug-Resistant Staphylococcus aureus Strains Reveal Distinct Biochemical Features with Raman Microspectroscopy. ACS Infect. Dis. 2018, 4 (8), 1197–1210. DOI: 10.1021/acsinfecdis.8b00029. [PubMed: 29845863]
42. Baig NF; Dunham SJB; Morales-Soto N; Shrout JD; Sweedler JV; Bohn PW, Multimodal Chemical Imaging of Molecular Messengers in Emerging Pseudomonas aeruginosa Bacterial Communities. Analyst 2015, 140, 6544–6552. [PubMed: 26331158]
43. Cao T; Sweedler JV; Bohn PW; Shrout JD, Spatiotemporal Distribution of Alkyl Quinolones in Pseudomonas aeruginosa Under Metabolic and Competitive Stress. mSphere 2020, 5, e00426–20. DOI: 10.1128/mSphere.00426-20. [PubMed: 32699119]
44. Perez-Vilar J; Hill RL, The Structure and Assembly of Secreted Mucins. J. Biol. Chem. 1999, 274 (45), 31751–31754. DOI: 10.1074/jbc.274.45.31751. [PubMed: 10542193]

45. Stayton PS; Olinger JM; Jiang M; Bohn PW; Sligar SG, Genetic engineering of surface attachment sites yields oriented protein monolayers. J. Am. Chem. Soc. 1992, 114 (24), 9298–9299. DOI: 10.1021/ja00050a008.

46. Hong HG; Bohn PW; Sligar SG, Optical determination of surface density in oriented metalloprotein nanostructures. Anal. Chem. 1993, 65 (11), 1635–1638. DOI: 10.1021/ac00059a025.

47. Gaifulina R; Maher AT; Kendall C; Nelson J; Rodriguez-Justo M; Lau K; Thomas GM, Label-free Raman spectroscopic imaging to extract morphological and chemical information from a formalin-fixed, paraffin-embedded rat colon tissue section. Int J Exp Pathol 2016, 97 (4), 337–350. DOI: 10.1111/iep.12194. [PubMed: 27581376]

48. Holloway BW, Genetic Recombination in Pseudomonas aeruginosa. Microbiology 1955, 13 (3), 572–581. DOI: 10.1099/00221287-13-3-572.

49. Heeb S; Fletcher MP; Chhabra SR; Diggle SP; Williams P; Cámara M, Quinolones: from antibiotics to autoinducers. FEMS Microbiol. Rev. 2011, 35 (2), 247–274. DOI: 10.1111/j.1574-6976.2010.00247.x. [PubMed: 20738404]

50. Barr HL; Halliday N; Barrett DA; Williams P; Forrester DL; Peckham D; Williams K; Smyth AR; Honeybourne D; J LW; Nash EF; Dewar J; Clayton A; Knox AJ; Camara M; Fogarty AW, Diagnostic and prognostic significance of systemic alkyl quinolones for P. aeruginosa in cystic fibrosis: A longitudinal study. J.Cyst. Fibros. 2017, 16 (2), 230–238. DOI: 10.1016/j.jcf.2016.10.005. [PubMed: 27773591]

51. Morales-Soto N; Dunham SJB; Baig NF; Ellis JF; Madukoma CS; Bohn PW; Sweedler JV; Shrout JD, Spatially dependent alkyl quinolone signaling responses to antibiotics in Pseudomonas aeruginosa swarms. J. Biol. Chem. 2018, 293 (24), 9544–9552. [PubMed: 29588364]

52. Baig N; Polisetti S; Morales-Soto N; Dunham SJ; Sweedler J; Shrout J; Bohn P, Label-free molecular imaging of bacterial communities of the opportunistic pathogen Pseudomonas aeruginosa. SPIE: 2016; Vol. 9930.

53. Polisetti S; Baig NF; Morales-Soto N; Shrout JD; Bohn PW, Spatial Mapping of Pyocyanin in Pseudomonas Aeruginosa Bacterial Communities Using Surface Enhanced Raman Scattering. Appl. Spectrosc. 2016, 71 (2), 215–223. DOI: 10.1177/0003702816654167. [PubMed: 27354400]

54. Pier GB; Coleman F; Grout M; Franklin M; Ohman DE, Role of Alginate O Acetylation in Resistance of Mucoid Pseudomonas aeruginosa to Opsonic Phagocytosis. Infect. Immun. 2001, 69 (3), 1895. DOI: 10.1128/IAI.69.3.1895-1901.2001. [PubMed: 11179370]

55. Li B; Comi TJ; Si T; Dunham SJB; Sweedler JV, A one-step matrix application method for MALDI mass spectrometry imaging of bacterial colony biofilms. J. Mass Spectrom. 2016, 51 (11), 1030–1035. DOI: 10.1002/jms.3827. [PubMed: 27476992]

56. Lanni EJ; Dunham SJB; Nemes P; Rubakhin SS; Sweedler JV, Biomolecular Imaging with a C60-SIMS/MALDI Dual Ion Source Hybrid Mass Spectrometer: Instrumentation, Matrix Enhancement, and Single Cell Analysis. J. Am. Soc. Mass. Spectrom. 2014, 25 (11), 1897–1907. DOI: 10.1021/jasms.8b04660. [PubMed: 25183225]

57. Bokhart MT; Nazari M; Garrard KP; Muddiman DC, MSiReader v1.0: Evolving Open-Source Mass Spectrometry Imaging Software for Targeted and Untargeted Analyses. J. Am. Soc. Mass. Spectrom. 2018, 29 (1), 8–16. DOI: 10.1021/jasms.8b05659. [PubMed: 28932998]

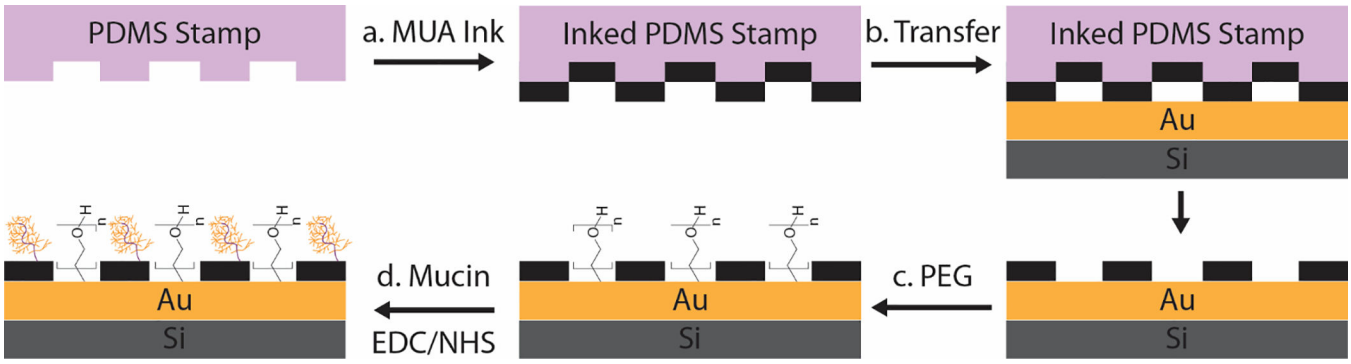

Figure 1.

Schematic illustration of the fabrication of mucin patterned surfaces. A patterned PDMS stamp is coated in MUA ink (a) and stamped on an Au-coated Si wafer (b). After the MUA stamp is applied, the remaining Au surface is coated with PEG to deter adventitious cell adhesion (c). Lastly, mucin is immobilized at the MUA pattern via EDC/NHS crosslinking (d).

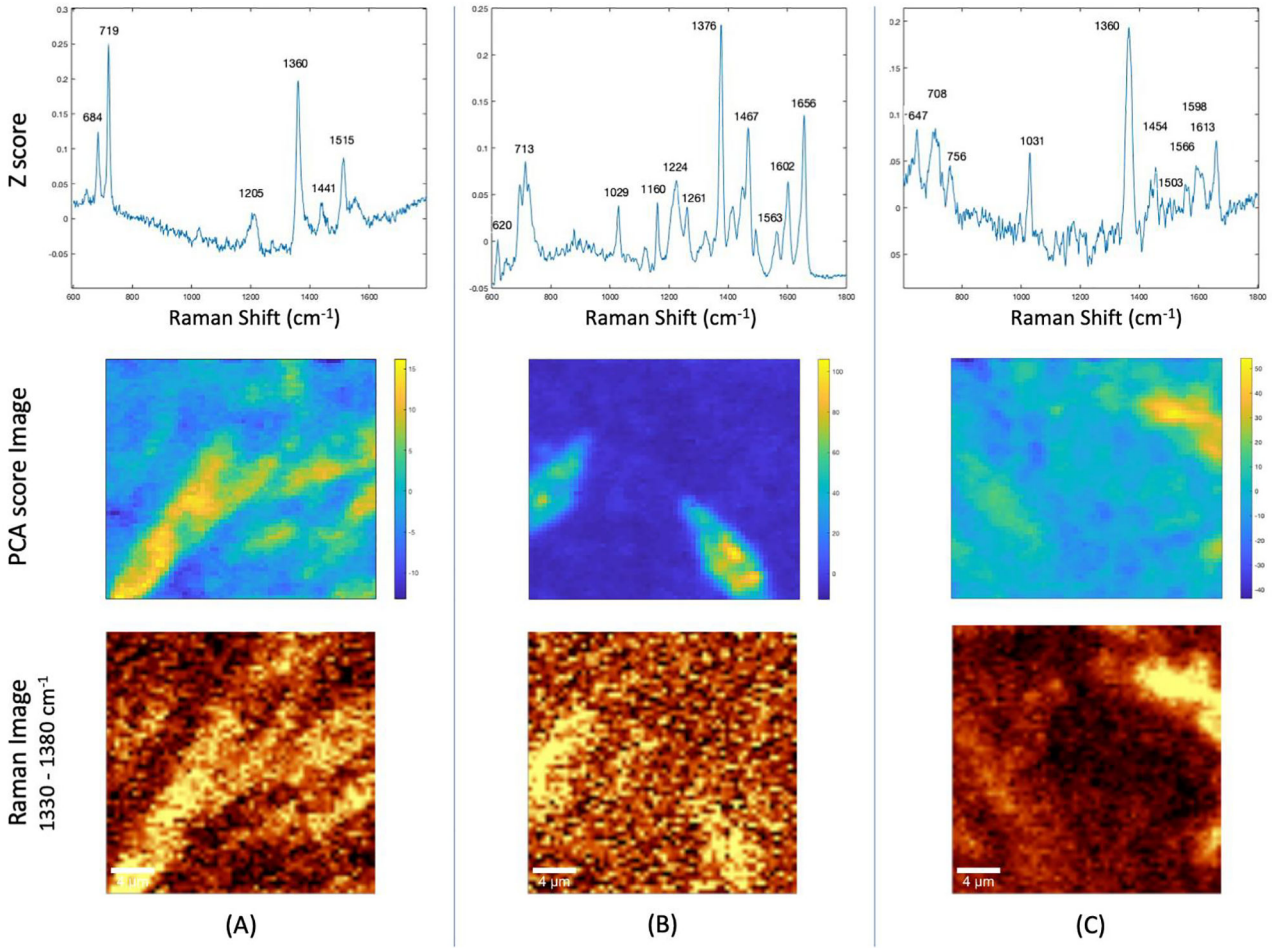

Figure 2. CRM imaging of *P. aeruginosa* surface adlayers shows multiple biomolecules.

(*Top row*) PCA loading plots showing the z-score *vs.* Raman shift for the highest ranking, chemically-relevant principal component. (*Middle row*) PCA score images show the spatial distribution and magnitude of the highest ranking, chemically-relevant principal component. (*Bottom row*) Raman images showing intensities integrated over 1330–1380 cm^{-1}. *Columns.* PCA loading plot, score images, and Raman intensity images in each column acquired from the same sample. (A) 24 h PAO1C biofilm on gold; PCA loading plot dominated by N/HQNO. (B) 48h PAO1C biofilm on mucin; loading plot dominated by PQS. (C) 48 h FRD1 biofilm on P-MUA; loading plot dominated by PYO.

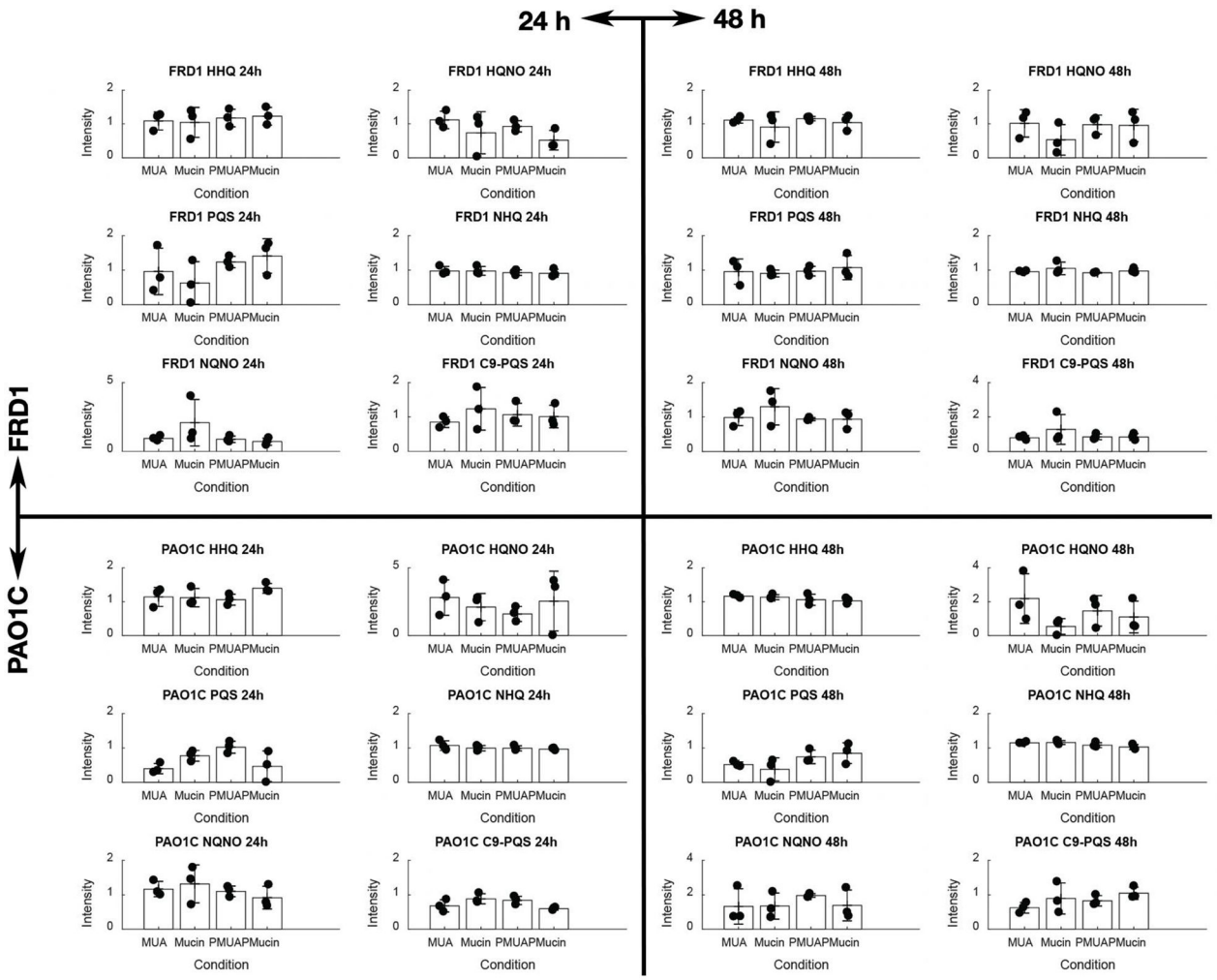

Figure 3. FRD1 and PAO1C biofilm variations in AQ relative AQ abundance with various surface modifications.

Histograms report the relative signal levels obtained from the MALDI MSI of different AQs produced by PAO1C and FRD1 *P. aeruginosa* strains grown for 24 h or 48 h on either unpatterned or patterned MUA or mucin.

Table 1.

Biomolecules detected by CRM [a, b]

	Strain	Gold	MUA	Mucin	P-MUA	P-Mucin
1–7 h	FRD1	Salt	Salt	Salt	Salt	Salt
	PAO1C	Salt	Salt	Salt	Salt	Salt
24 h	FRD1	PYO	HQNO	HQNO	Salt	HQNO
	PAO1C	HQNO	HQNO	HQNO	HQNO	HQNO
48 h	FRD1	PYO	HQNO, PQS, PYO	HQNO, PQS	HQNO, PYO	HQNO, PQS
	PAO1C	HQNO, PQS	HQNO, PQS	HQNO, PQS	HQNO, PQS	HQNO, PQS

[a]The presence of an entry for an AQ in the table indicates that PCA analysis of the images from this sample gave a Z-score plot matching the standard Raman spectrum of that component.

[b]HQNO and NQNO are indistinguishable by CRM, as are PQS and C9-PQS. Thus, entries for HQNO do not distinguish between the C7- and C9-congeners.